



Efficient C-band single-photon upconversion with chip-scale Ti-indiffused pp-LiNbO₃ waveguides

ZHENDA XIE,^{1,2,5} KAI HONG LUO,³ KAI CHI CHANG,^{2,6} NICOLAE C. PANOIU,⁴  HARALD HERRMANN,³ CHRISTINE SILBERHORN,³  AND CHEE WEI WONG^{1,2,7}

¹Optical Nanostructures Laboratory, Columbia University, New York, New York 10027, USA

²Fang Lu Mesoscopic Optics and Quantum Electronics Laboratory, University of California, Los Angeles, California 90095, USA

³Integrated Quantum Optics, Applied Physics, University of Paderborn, Warburger Str. 100, D-33098, Paderborn, Germany

⁴Department of Electronic and Electrical Engineering, University College London, Torrington Place, London WC1E 7JE, UK

⁵e-mail: xiezhenda@nju.edu.cn

⁶e-mail: uclakcchang@ucla.edu

⁷e-mail: cheewei.wong@ucla.edu

Received 30 April 2019; revised 27 June 2019; accepted 27 June 2019; posted 28 June 2019 (Doc. ID 366455); published 24 July 2019

Frequency upconversion for single photons at telecom wavelengths is important to simultaneously meet the different wavelength requirements for long-distance communications and quantum memories in a quantum nodal network. It also enables the detection for the telecom “flying qubit” photons with silicon-based efficient single-photon detectors with low dark count (DC) rates. Here, we demonstrate the frequency upconversion of attenuated single photons, using a low-loss titanium-indiffused periodically poled lithium niobate waveguide, pumped with a readily available erbium-doped fiber amplifier in the L-band. Internal and conversion efficiencies up to 84.4% and 49.9% have been achieved, respectively. The DC rates are suppressed down to 44 kHz at 13.9% end-to-end quantum efficiency (including full conversion and detection), enabled by our long-wavelength pump configuration and narrow 3.5-GHz bandpass filtering. © 2019 Optical Society of America

<https://doi.org/10.1364/AO.58.005910>

1. INTRODUCTION

In a proposed quantum optical communication network, non-classical photon sources are generated at different wavelengths for qubit-storage-versus-communication implementations. Two dominant wavelength ranges are: (1) the telecom wavelength with low absorption losses in optical fibers and (2) the visible/near-IR wavelengths between 600 nm and 895 nm for quantum memories. While the single photons at telecom wavelength are beneficial for long-distance quantum key distribution [1–4], visible/near-IR wavelengths are more compatible with the quantum memories [5–12] and detection systems.

Most quantum memories are based on photonic interactions with atomic transition, and they require the narrowband input at visible/near-IR wavelengths. These wavelengths are compatible with the single-photon detectors using silicon avalanche photodiodes, where the performance is superior to that conventional single-photon detectors made of InGaAs avalanche photodiodes with higher quantum efficiencies and lower dark count (DC) rates at telecom wavelength [13]. More recently, superconducting single-photon detectors also enable one of the highest quantum efficiencies and low DC rates, but they require cryogenic operation for a quantum network [14]. Single-photon frequency upconversion from the telecom

wavelength to visible/NIR wavelengths has been proposed as an efficient way to connect all the different devices working at different wavelengths [15]. It can be achieved by the sum-frequency generation (SFG) using a strong pump in a nonlinear optical medium [16–29]. Two approaches have been developed for more efficient SFG: one uses a bulk periodically poled lithium niobate (PPLN) crystal with a cavity enhancement [16–20], and the other one utilizes the reverse-proton-exchanged (RPE) PPLN waveguide [21–24]. Both schemes can achieve high conversion efficiency but the latter one requires a much lower pump power, and it is compatible with a future integrated quantum circuit as a waveguide device. However, the RPE PPLN waveguide only supports a TM mode, which limits the manipulation of polarization for single photons on a waveguide chip. On the other hand, the titanium-indiffused (Ti:) PPLN waveguide [30] supports both TE and TM modes [31–34], which can be a more ideal choice for future photonic integration involving the polarization degree of freedom.

2. EXPERIMENTAL RESULTS

For frequency upconversion at the single-photon level, residual (noise) photons from the strong pump may greatly increase the

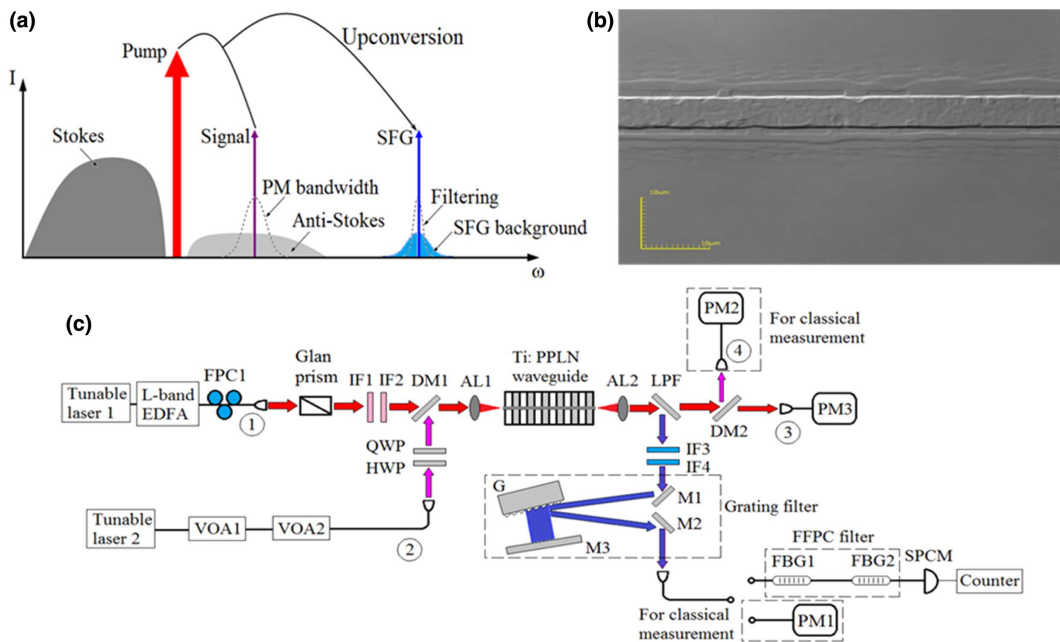


Fig. 1. (a) Schematic of the frequency upconversion. The SFG background can be generated from the residual noise photons of the strong pump light. The pump wavelength is set longer than the signal wavelength for the relatively weaker anti-Stokes scattering. Residual noise photons from within the phase-matching bandwidth contribute as background noise, to be reduced by narrowband filtering. (b) Microscope image of the PPLN waveguide chip. Scale bar: 10 nm. (c) Experiment setup. FPC, fiber polarization controller; IF, interference filter; DM, dichroic mirror; VOA, variable optical attenuator; HWP, half waveplate; QWP, quarter waveplate; AL, aspheric lens; LPF, long pass filter; M, mirror; G, ruled diffraction grating; PM, power meter; FPG, fiber Bragg grating; FFPC, fiber Fabry–Perot cavity; SPCM, single-photon counting module. AL1 is AR coated for 1050–1620 nm and AL2 is AR coated for 650–1050 nm. Optical power can be measured at points 1, 2, 3, and 4 for the transmission test. The grating filter and FFPC filter can be inserted to reduce the DC rate.

DC rate and reduce the signal-to-noise ratio, as shown in Fig. 1(a). These noise photons may result from Raman scattering and cascaded nonlinear parametric processes [23,24]. Previous studies show that the high DC rate can be reduced by narrowband spectral filtering from its broadband feature [22]. A very low DC rate has been achieved using monochromator filtering, with additional insertion loss from the monochromator. Besides narrowband filtering, it is beneficial to ensure that the pump wavelength is longer than the input signal because of the much lower probability of anti-Stokes emission than Stokes emission [22,23]. For a C-band input, a long-wavelength pump light source through an optical parametric oscillator has been implemented [23], including 2- μm fiber lasers [24]. Here, we present the measurements on the frequency upconversion of attenuated single photons from a telecom wavelength to a visible/NIR wavelength, using a 35-mm-long Ti:PPLN waveguide, with a commercially available L-band pump pump tunable laser and an erbium-doped fiber amplifier (EDFA) at 1570 nm. For the 1542.3–778-nm upconversion, an internal efficiency (pump photons to signal photons) and a conversion efficiency (signal photons to SFG photons) of up to 84.4% and 49.9% are measured, respectively. Efficient narrowband filtering has been achieved down to 3.5 GHz to maximize the signal-to-noise ratio. Here, we note that the 3.5-GHz filtering can be further improved by using narrower-band filter to be compatible for quantum memory application with typical tens of MHz of bandwidth. When tested with a single-photon detector based on silicon avalanche photodiodes, a 44-kHz DC

rate is achieved with a 13.9% quantum efficiency, which refers to the overall efficiency, including the conversion efficiency and the detection efficiency.

The Ti:PPLN waveguide used here has a poling period of 17.90 μm . Figure 1(b) shows the microscope image of the waveguide. The propagation loss of the waveguide has been measured by monitoring the interference fringes of the low Q cavity caused by the Fresnel reflection on its two facets with a 1550-nm tunable laser [35], and the loss is calculated to be 0.06 dB/cm, or 4.7% loss for a single pass through the waveguide. After this measurement, the input facet is anti-reflection (AR) coated with over 98% transmission from 1500 nm to 1700 nm, while the output facet is AR coated with over 98% transmission from 750 nm to 850 nm. The pump light comes from a tunable diode laser (Santec TSL-510) with its wavelength fixed at 1570 nm, as shown in the experimental scheme in Fig. 1(c). It is amplified by an L-band EDFA (Manlight HWT-EDFA-B-L-PM-33-1-FC/APC) to a maximum power of 2 W. A fiber polarization controller is used to change the input power. To make sure the pump is TM polarized before entering the Ti:PPLN waveguide, a Glan laser prism is used. Two narrowband interference filters (Semrock NIR01-1570/3-25) are cascaded to clean the pump light, with over 120 dB of rejection for the amplified spontaneous emission noise from the EDFA. The pump beam is then combined with the input signal on a dichroic mirror (DM1) before focusing into the Ti:PPLN waveguide. The single-photon signal is simulated by a weak coherent light source, which is from

another tunable diode laser with a tuning range from 1480 nm to 1580 nm (Ando AQ4321A). Two variable optical attenuators are connected in series to achieve over 120 dB of attenuation for the laser beam down to single-photon level. The Ti:PPLN waveguide is temperature stabilized in a homebuilt oven with an accuracy of 10 mK. The SFG output is separated by a long-pass filter from the pump and the remaining input. After passing through the filtering system, it can be detected by a power meter or a single-photon counting module (SPCM). The pump and remaining input are further separated by another dichroic mirror (DM2) and measured by two multi-mode-fiber coupled power meters respectively. The throughput coupling efficiency for the pump beam (from point 1 to point 3) and the signal beam (from point 2 to point 4) is measured to be 33.0% and 33.3%, which is reasonable compared to the calculated coupling efficiency of 59.5% and 60.0%, considering the reflection on the AR coatings at the output facet and the aspheric collimating lens at the output side (AL2). We then characterize the phase-matching of the Ti:PPLN waveguide. Figure 2(a) shows the far-field image of the fundamental TM mode. At 130°C, the SFG power is measured as a function of the signal wavelength [Fig. 2(b)]. The phase-matching wavelength is 1542.3 nm, and the full width half maximum is measured to be around 0.8 nm.

To describe the evolution of the mode amplitudes u_i upon mutual quasi-phase-matching interaction, we use the following system of equations for the SFG (denoted with subscript 3), the signal (denoted with subscript 2), and the pump (denoted with subscript 1) [36–39]:

$$i \frac{du_1}{dz} + \gamma_1 u_3 u_2^* e^{i\Delta\beta z} = 0, \quad (1a)$$

$$i \frac{du_2}{dz} + \gamma_2 u_3 u_1^* e^{i\Delta\beta z} = 0, \quad (1b)$$

$$i \frac{du_3}{dz} + \gamma_3 u_1 u_2 e^{-i\Delta\beta z} = 0, \quad (1c)$$

where $u_1(z)$, $u_2(z)$, and $u_3(z)$ are the mode amplitudes at the three frequencies and are measured in \sqrt{W} . The nonlinear parameters γ_i in the equations above are defined as

$$\gamma_1 = \frac{\epsilon_o \omega_1}{2\sqrt{P_1 P_2 P_3}} \int_{A_{nl}} dx dy \hat{e}_1^*(x, y; \omega_1) \cdot \hat{\chi}_{\text{eff}}(\omega_3, -\omega_2): \hat{e}_2^*(x, y; \omega_2) \hat{e}_3(x, y; \omega_3), \quad (2a)$$

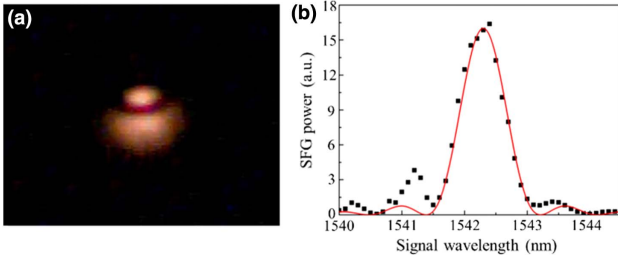


Fig. 2. (a) Far-field image of the TM_{01} mode. (b) Wavelength tuning curve at 130°C. The dots show the experimental results, and the peak SFG conversion can be achieved at a phase-matching wavelength of 1542.3 nm. The solid curve is a sinc square fit.

$$\gamma_2 = \frac{\epsilon_o \omega_2}{2\sqrt{P_1 P_2 P_3}} \int_{A_{nl}} dx dy \hat{e}_1^*(x, y; \omega_1) \cdot \hat{\chi}_{\text{eff}}(\omega_3, -\omega_2): \hat{e}_2^*(x, y; \omega_2) \hat{e}_3(x, y; \omega_3), \quad (2b)$$

$$\gamma_3 = \frac{\epsilon_o \omega_3}{2\sqrt{P_1 P_2 P_3}} \int_{A_{nl}} dx dy \hat{e}_1^*(x, y; \omega_1) \cdot \hat{\chi}_{\text{eff}}(\omega_3, -\omega_2): \hat{e}_2^*(x, y; \omega_2) \hat{e}_3(x, y; \omega_3), \quad (2c)$$

where A_{nl} is the nonlinear modal area and \hat{e}_i represents the modal E -fields. In addition, the normalization powers, P_i , the wave vector mismatch, $\Delta\beta$, and the waveguide effective susceptibility $\hat{\chi}_{\text{eff}}$ can be expressed as

$$P_i = \frac{1}{4} \int_S [\hat{e}_i(x, y) \times \hat{h}_i^*(x, y) + \hat{e}_i^*(x, y) \times \hat{h}_i(x, y)] \cdot \hat{z} dS \quad (3a)$$

$$i = 1, 2, 3,$$

$$\Delta\beta = \beta(\omega_3) - \beta(\omega_1) - \beta(\omega_2) - \frac{2\pi}{\Lambda} = \beta_3 - \beta_1 - \beta_2 - \frac{2\pi}{\Lambda}, \quad (3b)$$

$$\hat{\chi}_{\text{eff}} = \frac{2}{\pi} \hat{\chi}. \quad (3c)$$

Here, \hat{h}_i represents the modal H -fields. The resulting SFG quasi-phase-matching bandwidth is given by [40]

$$\delta\lambda = \frac{4\pi \cdot 0.4429}{L \left| \frac{\partial \Delta\beta}{\partial \lambda_2} \right|} = \frac{2 \cdot 0.4429 \lambda_2^2}{L |n_{g,2} - n_{g,3}|}, \quad (4)$$

where L is the length of the waveguide and $n_g = c/v_g$ is the group index, with v_g being the group velocity. Using the relation $P_i = W_i v_{g,i}$, where $W_i = \frac{1}{2} \int \epsilon(x, y) |\mathbf{e}_i(x, y)|^2 dx dy \equiv \frac{\epsilon_o \omega_i}{2}$ is the mode energy per unit length, the nonlinear parameters γ_i can be written as

$$\gamma_1 = \rho \omega_1 \int_{A_{nl}} dx dy \hat{e}_1^*(x, y; \omega_1) \cdot \hat{\chi}_{\text{eff}}(\omega_3, -\omega_2): \hat{e}_2^*(x, y; \omega_2) \hat{e}_3(x, y; \omega_3), \quad (5a)$$

$$\gamma_2 = \rho \omega_2 \int_{A_{nl}} dx dy \hat{e}_2^*(x, y; \omega_2) \cdot \hat{\chi}_{\text{eff}}(\omega_3, -\omega_1): \hat{e}_1^*(x, y; \omega_1) \hat{e}_3(x, y; \omega_3), \quad (5b)$$

$$\gamma_3 = \rho \omega_3 \int_{A_{nl}} dx dy \hat{e}_3^*(x, y; \omega_3) \cdot \hat{\chi}_{\text{eff}}(\omega_1, \omega_2): \hat{e}_1(x, y; \omega_1) \hat{e}_2(x, y; \omega_2). \quad (5c)$$

Here, $\rho = \sqrt{\frac{2}{\epsilon_o c^3} \frac{n_{g1} n_{g2} n_{g3}}{\omega_1 \omega_2 \omega_3}}$ is a frequency-independent coefficient. The resulting modeled SFG power versus pump power is shown in Fig. 3(d), with the power dependences versus waveguide distance shown in Fig. 3(d) inset. Without any fitting, the modeled SFG power is within the same order-of-magnitude and within 50% of the measured SFG power [Fig. 3(c)]. We also note that the numerical model used here does not

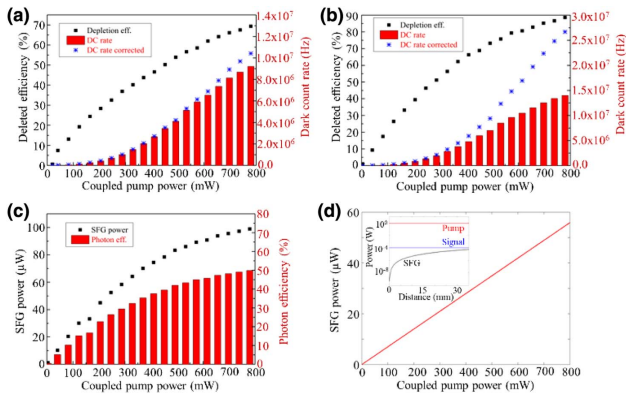


Fig. 3. (a) Depletion efficiency and DC rate measured at 30°C. (b) Depletion efficiency and DC rate measured at 130°C. (c) SFG power and photon efficiency measured with 100 μW signal input at 130°C. (d) Modeled SFG power versus coupled pump power. Inset: SFG and signal and pump powers versus distance at 800-mW pump power.

incorporate single-photon detector saturation, hence, the modeled SFG power is intrinsically linear with respect to the pump power. However, at a larger pump power, the theoretical model predicts a nonlinear dependence of SFG power on the pump power. In addition, the theory gives a phase-matching bandwidth of 0.65 nm, which is close to the experimental measurements, as shown in Fig. 2(b).

In measurements of Fig. 3, only a pair of cascaded interference filters is used, with an effective FWHM bandwidth of about 3 nm. As the residual noise photons from the pump are broadband, any noise photons that fall into this 3-nm bandwidth contribute as the dark count. Then, we reduce the filter bandwidth by using a high-efficiency ruled grating, as shown in Fig. 1(c). A double-pass configuration is used to reduce the filtering bandwidth down to 21.5 GHz. The transmission of this filtering system is measured to be 52.0%, which is mainly limited by the grating efficiency of 76%.

We perform the single-photon upconversion test with an input-photons flux at 1 MHz. The quantum efficiency and the DC rate can be calculated by monitoring the upconversion counting rate from the SPCM, which is shown in Fig. 4. The maximum quantum efficiency is 15.6% with a DC rate of 289 kHz at 30°C, while it corresponds to 19.5% with a DC rate of 550 kHz at 130°C. The DC rate is reduced by 16.9 dB compared to the case which only applies a pair of 3-nm effective bandwidth cascaded interference filters. Moreover, we can reduce the DC rate with narrower filtering with a fiber Fabry–Perot cavity (FFPC).

The FFPC is formed on a 780-nm single-mode fiber by two fiber Bragg gratings (FBG) with a separation of 820 μm, which corresponds to a free spectral range (FSR) of 124 GHz. After combining with the grating filter, only one transmission peak is selected with 91% transmittance. The two FBGs are made with effective FWHM bandwidths of 2 nm and centered at 778 nm, which matches well with the SFG wavelength at 130°C. Our FFPC has finesse of 36 and a transmission FWHM bandwidth of 3.5 GHz. As shown in Fig. 4(c), the DC rate can be further suppressed by 27.8 dB to 44 kHz at a maximum quantum

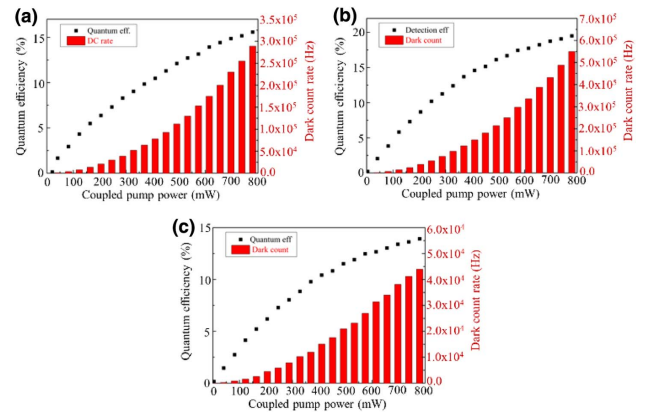


Fig. 4. (a) Quantum efficiency and DC rate measured with grating filter at 30°C. (b) Quantum efficiency and DC rate measured with grating filter at 130°C. (c) Quantum efficiency and DC rate measured with grating and FFPC filters at 130°C.

efficiency of 13.9%, compared to the case with cascaded interference filters of 3-nm effective bandwidth. We note that the DC rate is still high even with a 3.5-GHz filtering, which is probably coming from the Lorentzian tail of the pump laser at 1570 nm, since the center of the signal wavelength is only 28 nm away from the pump. The lower efficiency is mainly due to the mode mismatch between the 780 nm single mode fiber and the TM_{01} mode for the SFG light from the Ti:PPLN waveguide. By optimizing the mode matching to the SFG light with the TM_{00} mode, higher single-mode-fiber coupling efficiency can be expected.

3. CONCLUSIONS

In conclusion, we have demonstrated single-photon-level frequency upconversion from a telecom wavelength to a NIR/visible wavelength using a Ti:PPLN waveguide. Here, we only investigate the TM mode of the Ti:PPLN waveguide to avoid the complexity of analyzing the upconversion results. The polarization independence of the Ti:PPLN will be investigated in our future work. It is shown that the Ti:PPLN waveguide can realize efficient frequency upconversion. This result can be important for the future integrated quantum circuit because of its potential operation on the polarization degree of freedom at single-photon level. An 84.4% internal efficiency and a 49.9% conversion efficiency have been achieved for the C-band input at 1542.3 nm. Efficient narrowband filtering down to 3.5 GHz has been realized by cascading a double-pass grating system with a FFPC, which greatly reduces the DC rate by 27.8 dB, compared to the case with cascaded interference filters of a 3-nm effective bandwidth. After such filtering, a maximum quantum efficiency of 13.9% has been measured using a SPCM with a 72% detection efficiency, and the DC rate is 44 kHz in this case.

In this work, the coupled pump power is about 800 mW to achieve high conversion efficiency, which is one of the main reasons for the high DC rate without filtering. After filtering, our system still has a relatively high DC rate. Improvements such as a larger wavelength difference between the pump

and the signal photons, a longer waveguide, narrower bandpass filtering, and better poling quality are under development. Compared to other existing schemes for single-photon-level up-conversion, our narrowband filtering method has an internal upconversion efficiency already at 49.9% (13.9% end-to-end quantum efficiency); with narrower filtering bandwidth down to tens of MHz, our Ti:PPLN waveguide upconversion approach would be directly relatable to existing quantum memory systems at telecom wavelengths.

Funding. Defense Advanced Research Projects Agency (DARPA) (D133-001-0076); University of California National Laboratory research program (LFRP-17-477237); Office of Naval Research (ONR) (N00014-14-1-0041); Lawrence Livermore National Laboratory (LLNL) (B622827).

Acknowledgment. The authors acknowledge funding support from DARPA Defense Science Office under Dr. Prem Kumar.

REFERENCES

- C. Gobby, Z. L. Yuan, and A. J. Shields, "Quantum key distribution over 122 km of standard telecom fiber," *Appl. Phys. Lett.* **84**, 3762–3764 (2004).
- P. Zhang, K. Aungskunsiri, E. Martín-López, J. Wabnig, M. Lobino, R. W. Nock, J. Munns, D. Bonneau, P. Jiang, H. W. Li, A. Laing, J. G. Rarity, A. O. Niskanen, M. G. Thompson, and J. L. O'Brien, "Reference frame independent quantum key distribution server with telecom tether for on-chip client," *Phys. Rev. Lett.* **112**, 130501 (2014).
- P. Jouguet, S. Kunz-Jacques, A. Leverrier, P. Grangier, and E. Diamanti, "Experimental demonstration of long-distance continuous-variable quantum key distribution," *Nat. Photonics* **7**, 378–381 (2013).
- S. Wang, Chen, J.-F. Guo, Z.-Q. Yin, H.-W. Li, Z. Zhou, G.-C. Guo, and Z.-F. Han, "2 GHz clock quantum key distribution over 260 km of standard telecom fiber," *Opt. Lett.* **37**, 1008–1010 (2012).
- B. Julsgaard, J. Sherson, J. I. Cirac, J. Fiurasc, and E. S. Polzik, "Experimental demonstration of quantum memory for light," *Nature* **432**, 482–486 (2004).
- W. Rosenfeld, S. Berner, J. Volz, M. Weber, and H. Weinfurter, "Remote preparation of an atomic quantum memory," *Phys. Rev. Lett.* **98**, 050504 (2007).
- G. Hetet, J. J. Longdell, A. L. Alexander, P. K. Lam, and M. J. Sellars, "Electro-optic quantum memory for light using two-level atoms," *Phys. Rev. Lett.* **100**, 023601 (2008).
- T. Chaneliere, D. N. Matsukevich, S. D. Jenkins, S. Y. Lan, T. A. B. Kennedy, and A. Kuzmich, "Storage and retrieval of single photons transmitted between remote quantum memories," *Nature* **438**, 833–836 (2005).
- K. S. Choi, H. Deng, J. Laurat, and H. J. Kimble, "Mapping photonic entanglement into and out of a quantum memory," *Nature* **452**, 67–71 (2008).
- S. Tanzilli, W. Tittel, M. Halder, O. Alibart, P. Baldi, N. Gisin, and H. Zbinden, "A photonic quantum information interface," *Nature* **437**, 116–120 (2005).
- M. Bock, P. Eich, S. Kucera, M. Kreis, A. Lenhard, C. Becher, and J. Eschner, "High-fidelity entanglement between a trapped ion and a telecom photon via quantum frequency conversion," *Nat. Commun.* **9**, 1998 (2018).
- D. D. Awschalom, R. Hanson, J. Wrachtrup, and B. B. Zhou, "Quantum technologies with optically interfaced solid-state spins," *Nat. Photonics* **12**, 516–527 (2018).
- R. H. Hadfield, "Single-photon detectors for optical quantum information applications," *Nat. Photonics* **3**, 696–705 (2009).
- R. Valivarthi, Q. Zhou, G. H. Aguilar, V. B. Verma, F. Marsili, M. D. Shaw, S. W. Nam, D. Oblak, and W. Tittel, "Quantum teleportation across a metropolitan fibre network," *Nat. Photonics* **10**, 676–680 (2016).
- P. Kumar, "Quantum frequency conversion," *Opt. Lett.* **15**, 1476–1478 (1990).
- M. A. Albota and F. N. C. Wong, "Efficient single-photon counting at 1.55 μm by means of frequency upconversion," *Opt. Lett.* **29**, 1449–1451 (2004).
- H. Pan, E. Wu, H. Dong, and H. Zeng, "Single-photon frequency up-conversion with multimode pumping," *Phys. Rev. A* **77**, 033815 (2008).
- H. Pan, H. Dong, H. Zeng, and W. Lu, "Efficient single-photon counting at 1.55 μm by intracavity frequency upconversion in a unidirectional ring laser," *Appl. Phys. Lett.* **89**, 191108 (2006).
- H. Pan and H. Zeng, "Efficient and stable single-photon counting at 1.55 μm by intracavity frequency upconversion," *Opt. Lett.* **31**, 793–795 (2006).
- C. E. Vollmer, C. Baune, A. Sambrowski, T. Eberle, V. Händchen, J. Fiurásek, and R. Schnabel, "Quantum up-conversion of squeezed vacuum states from 1550 to 532 nm," *Phys. Rev. Lett.* **112**, 073602 (2014).
- L. Ma, O. Slattery, and X. Tang, "Single photon frequency up-conversion and its applications," *Phys. Rep.* **521**, 69–94 (2012).
- L. Ma, J. C. Bienfang, O. Slattery, and X. Tang, "Up-conversion single-photon detector using multi-wavelength sampling techniques," *Opt. Express* **19**, 5470–5479 (2011).
- J. S. Pelc, Ma, C. R. Phillips, Q. Zhang, C. Langrock, O. Slattery, X. Tang, and M. M. Fejer, "Long-wavelength-pumped upconversion single-photon detector at 1550 nm: performance and noise analysis," *Opt. Express* **19**, 21445–21456 (2011).
- G. L. Shentu, X. X. Xia, Q. C. Sun, J. S. Pelc, M. M. Fejer, Q. Zhang, and J. W. Pan, "Upconversion detection near 2 μm at the single photon level," *Opt. Lett.* **38**, 4985–4987 (2013).
- C. Langrock, E. Diamanti, R. V. Roussev, Y. Yamamoto, and M. M. Fejer, "Highly efficient single-photon detection at communication wavelengths by use of upconversion in reverse-proton-exchanged periodically poled LiNbO₃ waveguides," *Opt. Lett.* **30**, 1725–1727 (2005).
- M. T. Rakher, L. Ma, O. Slattery, X. Tang, and K. Srinivasan, "Quantum transduction of telecommunications-band single photons from a quantum dot by frequency upconversion," *Nat. Photonics* **4**, 786–791 (2010).
- N. K. Langford, S. Ramelow, R. Prevedel, W. J. Munro, G. J. Milburn, and A. Zeilinger, "Efficient quantum computing using coherent photon conversion," *Nature* **478**, 360–363 (2011).
- C. J. McKinstrie, M. Yu, M. G. Raymer, and S. Radic, "Quantum noise properties of parametric processes," *Opt. Express* **13**, 4986–5012 (2005).
- D. Shayovitz, H. Herrmann, W. Sohler, R. Ricken, C. Silberhorn, and D. M. Marom, "Time-to-space conversion of ultrafast waveforms at 1.55 μm in a planar periodically poled lithium niobate waveguide," *Opt. Lett.* **38**, 4708–4711 (2013).
- M. Mohageg, A. B. Matsko, and L. Maleki, "Lasing and up conversion from a nominally pure whispering gallery mode resonator," *Opt. Express* **20**, 16704–16714 (2012).
- Q. Zheng, H. Zhu, S.-C. Chen, C. Tang, E. Ma, and X. Chen, "Frequency-upconverted stimulated emission by simultaneous five-photon absorption," *Nat. Photonics* **7**, 234–239 (2013).
- O. Kuzucu, F. N. C. Wong, S. Kurimura, and S. Tovstonog, "Time-resolved single-photon detection by femtosecond upconversion," *Opt. Lett.* **33**, 2257–2259 (2008).
- H. Takesue, K. Inoue, O. Tadanaga, Y. Nishida, and M. Asobe, "Generation of pulsed polarization-entangled photon pairs in a 1.55- μm band with a periodically poled lithium niobate waveguide and an orthogonal polarization delay circuit," *Opt. Lett.* **30**, 293–295 (2005).
- A. Martin, A. Issautier, H. Herrmann, W. Sohler, D. B. Ostrowsky, O. Alibart, and S. Tanzilli, "A polarization entangled photon-pair source based on a type-II PPLN waveguide emitting at a telecom wavelength," *New J. Phys.* **12**, 103005 (2010).
- G. Fujii, N. Namekata, M. Motoya, S. Kurimura, and S. Inoue, "Bright narrowband source of photon pairs at optical telecommunication

- wavelengths using a type-II periodically poled lithium niobate waveguide," *Opt. Express* **15**, 12769–12776 (2007).
36. K. H. Luo, H. Herrmann, S. Krapick, R. Ricken, V. Quiring, H. Suche, W. Sohler, and C. Silberhorn, "Two-color narrowband photon pair source with high brightness based on clustering in a monolithic waveguide resonator," arXiv:1306.1756 (2013).
 37. R. Regener and W. Sohler, "Loss in low-finesse Ti:LiNbO₃ optical waveguide resonators," *Appl. Phys. B* **36**, 143–147 (1985).
 38. M. M. Fejer, G. A. Magel, D. H. Jundt, and R. L. Byer, "Quasi-phase-matched second harmonic generation: tuning and tolerances," *IEEE J. Quantum Electron.* **28**, 2631–2654 (1992).
 39. N. C. Panoiu, R. M. Osgood, and B. A. Malomed, "Semidiscrete composite solitons in arrays of quadratically nonlinear waveguides," *Opt. Lett.* **31**, 1097–1099 (2006).
 40. N. C. Panoiu, B. A. Malomed, and R. M. Osgood, "Semidiscrete solitons in arrayed waveguide structures with Kerr nonlinearity," *Phys. Rev. A* **78**, 013801 (2008).